

Rheological Characterization of Magnetorheological Fluids for Brake Applications: An Experimental Procedure

*Original*

Rheological Characterization of Magnetorheological Fluids for Brake Applications: An Experimental Procedure / Peruzzi, G., Imberti, G., De Carvalho Pinheiro, H., Tsantilis, L., Sethi, R., Santagata, E.. - In: FLUIDS. - ISSN 2311-5521. - 10:2(2025), pp. 1-19. [10.3390/fluids10020050]

*Availability:*

This version is available at: 11583/2999269 since: 2025-04-16T14:59:40Z

*Publisher:*

Multidisciplinary Digital Publishing Institute (MDPI)

*Published*

DOI:10.3390/fluids10020050




*Terms of use:*

This article is made available under terms and conditions as specified in the corresponding bibliographic description in the repository

*Publisher copyright*

(Article begins on next page)

# Rheological Characterization of Magnetorheological Fluids for Brake Applications: An Experimental Procedure

Guglielmo Peruzzi <sup>1</sup>, Giovanni Imberti <sup>1,\*</sup>, Henrique de Carvalho Pinheiro <sup>1,\*</sup> , Lucia Tsantilis <sup>2</sup> ,  
Rajandrea Sethi <sup>2</sup>  and Ezio Santagata <sup>2,3</sup>

- <sup>1</sup> Department of Mechanical and Aerospace Engineering DIMEAS, Politecnico di Torino, 10129 Torino, Italy; guglielmo.peruzzi@polito.it  
<sup>2</sup> Department of Environment, Land and Infrastructure Engineering DIATI, Politecnico di Torino, 10129 Torino, Italy; lucia.tsantilis@polito.it (L.T.); rajandrea.sethi@polito.it (R.S.); ezio.santagata@qu.edu.qa (E.S.)  
<sup>3</sup> Department of Civil and Environmental Engineering, Qatar University, Doha P.O. Box 2713, Qatar  
\* Correspondence: giovanni.imberti@polito.it (G.I.); henrique.decarvalho@polito.it (H.d.C.P.)

**Abstract:** This work focused on the development of a complete laboratory procedure for the rheological characterization of magnetorheological fluids (MRFs) by combining information gained from the literature and practical work performed in the laboratory. The procedure developed involves all the experimental stages for a comprehensive analysis, starting from the sample preparation, choice of the optimal measuring system, definition of the test, and rheometric parameters for the execution of an accurate and reliable analysis. Magnetorheology is a critical approach for studying the field-dependent properties of MRFs; however, measurement errors, often stemming from inappropriate rheometric test parameters, pose significant challenges. Additionally, sedimentation, caused by the large density mismatch between magnetic particles and the carrier fluid, presents a major obstacle that can compromise the analysis. Extensive work was performed for selecting the test parameters as well as defining the most relevant type of analysis to conduct with the defined procedure for the definition of the essential properties of an MRF for braking applications. This work is essential for the development of accurate card material for simulation tools, paving the way for broader utilization of MRFs in cutting-edge technologies.



Academic Editor: Sergey Smolentsev

Received: 23 December 2024

Revised: 31 January 2025

Accepted: 7 February 2025

Published: 13 February 2025

**Citation:** Peruzzi, G.; Imberti, G.; de Carvalho Pinheiro, H.; Tsantilis, L.; Sethi, R.; Santagata, E. Rheological Characterization of Magnetorheological Fluids for Brake Applications: An Experimental Procedure. *Fluids* **2025**, *10*, 50. <https://doi.org/10.3390/fluids10020050>

**Copyright:** © 2025 by the authors. Licensee MDPI, Basel, Switzerland. This article is an open access article distributed under the terms and conditions of the Creative Commons Attribution (CC BY) license (<https://creativecommons.org/licenses/by/4.0/>).

**Keywords:** magnetorheological fluid; characterization; magnetorheology; automotive; brake

## 1. Introduction

Magnetorheological fluids (MRFs) are a class of smart materials that exhibit remarkable and controllable changes in their rheological properties when subjected to an external magnetic field. The primary mechanism behind this transformation is the alignment of ferromagnetic or paramagnetic particles suspended in a carrier fluid, which form chain-like structures in response to a magnetic field [1] in a few milliseconds (typically between 0.8 ms and 6 ms) [2,3]. This rapid structural transformation results in a significant increase in the fluid's viscosity, allowing complete control over the torque transmission [4]. The complete reversibility of the magnetorheological (MR) effect and responsiveness of MRFs to magnetic fields have led to their widespread use in various applications, particularly in adaptive systems such as dampers, clutches, brakes, and actuators [5–9].

MRFs consist of micron-sized ferromagnetic particles, typically iron or iron alloys, dispersed in a non-magnetic carrier fluid such as silicone or mineral oil. The particles are usually coated with a stabilizing agent to prevent agglomeration or settling in the absence

of a magnetic field [10]. When no magnetic field is applied, the MRF behaves similarly to a Newtonian or weakly non-Newtonian fluid, with low yield stress and moderate viscosity. However, upon exposure to a magnetic field, the magnetic dipoles of the suspended particles align along the direction of the magnetic field, forming chains and structures that significantly alter the fluid's rheological properties. This alignment increases the material's resistance to flow, leading to a rise in yield stress and viscosity.

The key characteristics of MRFs is their controllable viscosity, which can be tuned by varying the intensity of the applied magnetic field. By adjusting the strength of the magnetic field, the fluid can transition between its liquid-like and solid-like states in milliseconds, as shown in Figure 1, thus providing fast and precise control over mechanical resistance fundamental for an electro-actuated system [1,6,11,12].

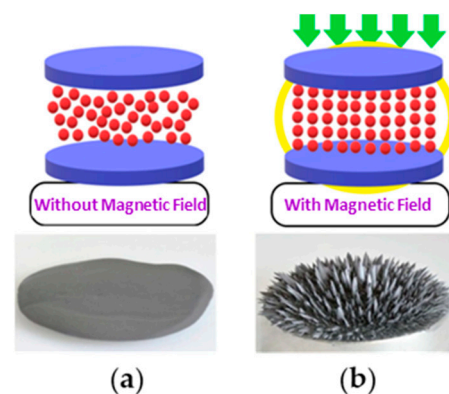


**Figure 1.** MRF particles distribution under (a) no external magnetic field; (b) with the external field. Adapted from [11].

MR devices, such as brakes and clutches, utilize the MR effect in direct shear mode, where the MRF is positioned between a stator and rotor and generates torque that resists the applied shear. This torque provides the controllable resistance needed for braking or clutching operations [13]. In this case, the field is applied perpendicular to the shearing forces and the particles align along the field, forming chain-like structures in static condition that increase the mechanical resistance to the fluid flow. Figure 2 illustrates the structure generated by the field while a shearing force is applied. In scenario (a), when the MRF is in an equilibrium state and a force is applied, the resulting deformation initially stays below the fluid's yield point. This means the force is still not strong enough to break the magnetic particle chains initially formed. Instead, these chains, aligned along the magnetic field, elongate, maintaining the structured network. In scenario (b), once the applied force exceeds the static yield point of the magnetized fluid, the particle chains break. As a result, the fluid's internal structure transitions from these chain-like formations to lamellar (layered) structures, which then continue to break and reform under continued shearing. The fluid is still able to resist motion and produce torque, even though its solid-like structure is continually disrupted and rebuilt during the shearing process. This dynamic behavior is critical for applications like brakes, where the MRF must provide consistent resistance during motion and at rest conditions.

The performance of a magnetorheological fluid (MRF) is primarily defined by its maximum yield stress, which directly reflects the strength of the particle structures formed when a magnetic field is applied [14]. However, an MRF's effectiveness cannot be judged solely by its yield stress. Several other factors are critical for optimal performance in a braking application, such as colloidal stability, which ensures the fluid maintains its functionality over time without particle settling. Low off-state viscosity is essential to minimize residual rolling resistance when the brake is not engaged. High-temperature

stability is also crucial, as braking generates significant heat. The base fluid must resist thermal degradation within the operating temperature range, and the fluid’s on-state properties must remain stable to guarantee the system’s reliability and safety under all conditions [15].

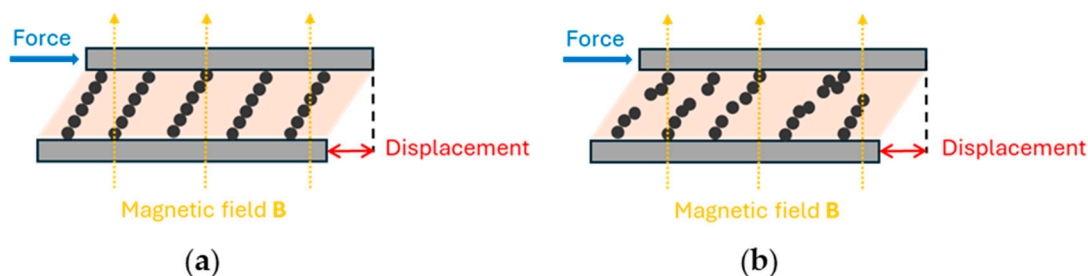


**Figure 2.** (a) Shear force acting on a magnetized MRF in the pre-yield deformation region; (b) overcoming of the yielding point breaking of the particle chains with the formation of clusters.

This research article introduces a standardized methodology for performing essential rheological tests to identify key MRF parameters such as the minimum viscosity at the off state and the yield stress at different magnetization and viscosity variations across the ranges of shear rates. These are critical aspects for optimizing the braking performance. The methodology was developed through a rigorous review of the most significant studies in MRF rheology, expanded by defining specific rheometric parameters obtained from extensive experimental work. The current literature lacks a comprehensive methodology for the exhaustive characterization of MR fluids, though specific tests are discussed in various articles. For instance, off-state measurements are presented in [10,13], where the cone-plate geometry is also introduced. On-state flow curves are detailed in [5,16–19], which describe the concept of pre-shearing and steady-state measurements. Controlled shear stress experiments are covered in [19,20], and temperature-dependent tests are thoroughly reviewed in [21,22]. However, in many of these publications, the rheometric parameters are not consistently defined, and the tests are often limited to low shear rate regimes. Despite these limitations, these studies have been instrumental in laying the groundwork for the development of a more complete characterization methodology.

Particular emphasis was placed also on examining the material’s properties’ dependency on different working conditions such as temperature, gap height, shear rate, and magnetic field strength, factors crucial for the optimization of braking system design and performance [23–26]. Based on the so-defined methodology, the characterization of a commercial MRF was performed to understand if it is a good candidate material for magnetorheological brake system applications.

## 2. Materials and Methods

### 2.1. MRF Sample

For this article, a commercial MRF was used for testing. We tested whether the properties declared by the producer, presented in Table 1, meet minimum requirements that an MRF for brake applications should satisfy. These parameters were identified in this study as an off-state viscosity below 500 mPa·s, a yield stress above 45 kPa, and an operational temperature range from −40 °C to 140 °C.

**Table 1.** Main parameters of the commercially available MRF.

Viscosity	Density	Particle wt%	Temperature Range
0.112 Pa·s (@40 °C)	2.95–3.13 g/cm <sup>3</sup>	80.98%	−40 to 130 °C

## 2.2. Experimental Setup

The on- and off-state rheological properties of the MRF were studied with an Anton Paar MCR 301, Graz, Austria in different measurement configurations. For the characterization under application of magnetic field, the rheometer was equipped with an MRD-70/1T magnetocell (Anton Paar) equipped with a parallel-plate spindle geometry, as shown in Figure 3. The validation of the measuring geometry as well as the homogeneity of the field generated is well established by many authors [16,17,27]. The cell allows the generation of a homogeneous field up to 1 T in the region between the measuring plates, facilitated by an upper yoke that efficiently closes the magnetic circuit in close proximity to the plate.

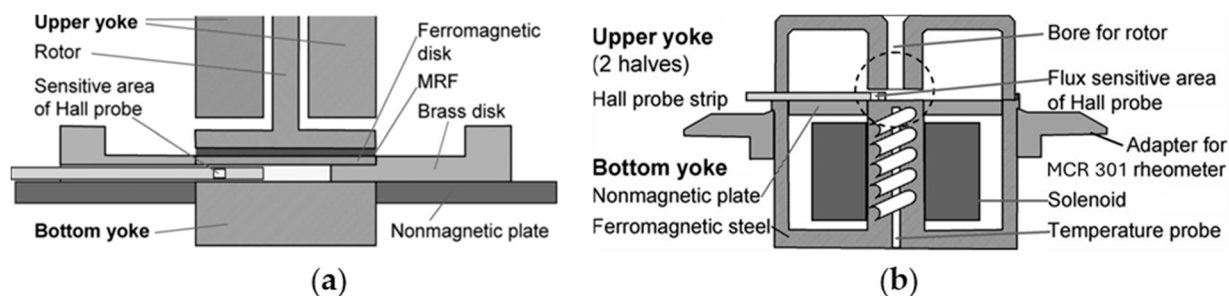


**Figure 3.** Schematics of the magnetocell developed by Anton Paar for rheological characterization of field-sensitive materials, adapted from [27]. (a) Parallel-plate insert with the slot for online measurements of the magnetic field and (b) schematics of the induction coils and top yoke for closing the magnetic circuit on top of the sample plate.

Temperature control is achieved by a thermocirculator, namely the LAUDA Ecoline RE 207 (Königshofen, Germany), which allows regulation across a wide range of temperatures ( $-30\text{ }^{\circ}\text{C}$  to  $90\text{ }^{\circ}\text{C}$ ). For the tests, however, since the magnetocell has an upper limit of  $70\text{ }^{\circ}\text{C}$ , a working temperature range from  $10\text{ }^{\circ}\text{C}$  to  $65\text{ }^{\circ}\text{C}$  was selected.

## 2.3. Sample Preparation

To ensure homogeneity and prevent errors caused by potential sedimentation, the MRF was thoroughly stirred for 5 to 10 min using a standard laboratory mixer before each experiment. It is worth noting that the re-homogenization of the material was performed at a low rotational speed of 1400 rpm to prevent excessive local heating formation that could be detrimental to the fluid properties. Furthermore, low speed was maintained also to avoid damage to the particles caused by the rotor blades. The definition of adequate homogeneity conditions was based on visual inspection of the fluid container by verifying that no sedimentation of particles could be detected at the bottom. This step was taken to eliminate any density mismatches and ensure consistent fluid properties during each analysis. Even minor variations in the concentration of metal particles can lead to significant changes in the rheological properties of the fluid, potentially invalidating the analysis.

For a precise fluid volume control during the analysis and to improve test repeatability, a volume-controlled micropipette ( $1000\text{--}100\text{ }\mu\text{L}$ ) was used to accurately dispense the exact required amount of MRF. Due to the tacky nature of the base oil, special care must be taken during pipette operation. The reverse pipetting method was employed to ensure proper release of the fluid, as it minimizes errors caused by adhesion to the pipette tip, allowing for consistent and accurate volume delivery. For this approach, the depress plunger is pressed completely, and the MRF is withdrawn and then released by pressing the plunger up to the first stop. In this way, a small volume of fluid remains in the tip, acting as a piston pushing the fluid. The variation in fluid volume between withdrawals was reduced to just  $3\text{--}5\text{ }\mu\text{L}$ , which is negligible and does not significantly affect the accuracy or consistency of the analysis results.

#### 2.4. Choice of the Measuring System

On-state measurements were conducted using a parallel-plate geometry with a diameter of 20 mm, at a gap height of 1 mm, and a fluid volume of 400  $\mu\text{L}$ , which exceeds the maximum theoretical gap volume of 314  $\mu\text{L}$ . During several failed tests, it was observed that the use of the exact theoretical volume often caused the fluid to escape from the gap. This occurred due to the low viscosity of the MRF's base oil, which made the fluid flatten out, thus avoiding proper contact between the plates. The slight excess in fluid volume was necessary to maintain consistent contact and ensure accurate measurement. The choice of the gap was based on findings from previous studies on magnetorheological braking (MRB) systems, which demonstrated that a gap between 1 mm and 2 mm provides optimal performance in an MRB. Gaps larger than 2 mm result in weaker magnetic particle structures, reducing the braking torque generated and compromising performance. Conversely, reducing the gap below 1 mm leads to excessive rolling resistance, hindering the system's efficiency. Therefore, the selected range ensures a balance between strong magnetic structures for adequate torque and manageable rolling resistance for smoother operation [6,18,28]. Above 1 mm, it was found to be impossible to perform any analysis, as there was no proper contact between the fluid and the rotating plate, while at lower gaps, analyses were conducted to study the effect of increasing resistance.

Off-state measurements were performed with both the magnetocell equipped with the parallel-plate system and a traditional cone-plate system (without the magnetocell) with a cone angle of  $0.998^\circ$ , a diameter of 50 mm, and a fixed gap at the cone truncation of 0.1 mm; both systems are represented in Figure 4. The main advantage of the cone-plate system is that it generates a homogeneous shear rate across the sample, as the velocity gradient in the radial direction is constant. Conversely, for a parallel-plate system, the shear rate increases radially, requiring data correction for a reliable evaluation of the shear stress, yield stress, and viscosity parameters. One important aspect to consider is the particle dimension with respect to the gap height for the type of measuring system chosen. Particle dimensions should be at least ten times smaller than the gap to ensure optimal working conditions and to avoid any possible damage induced to the system.

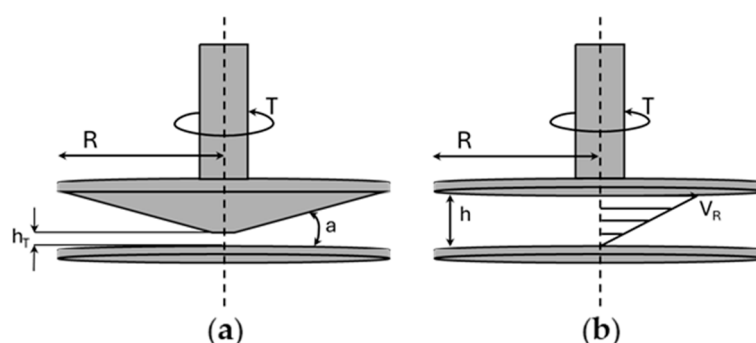


**Figure 4.** Diagram of the two measuring systems used for the rheological characterization: (a) cone-plate (CP) system; (b) parallel-plate (PP) system.  $R$ , radius;  $T$ , torque;  $h$ , gap height;  $h_T$ , cone truncation gap;  $a$ , cone angle; and  $V_R$ , velocity gradient.

#### 2.5. Characterization Procedure and Definition of Rheometric Parameters

Three kinds of test were conducted to determine the material properties' dependencies on variations in temperature, gap height, fluid volume, field intensity, and shear rate. Each of these parameters plays a crucial role in determining the fluid's behavior under operational conditions and its suitability for specific conditions.

1. Flow curve measurements in off-state conditions were performed to study the behavior of shear stress and viscosity as a function of temperature and gap height.

The tests were performed with both the PP and CP system, so the test procedure is valid for both systems. Prior to measurements, the fluid was sheared for 1 min at  $20 \text{ s}^{-1}$  to eliminate any possible shear history effect and then left for 1 min to reach an equilibrium state prior to the analysis. The test was then evaluated by step increasing the shear rate logarithmically from  $1 \text{ s}^{-1}$  to  $1000 \text{ s}^{-1}$  with a time setting of 20 Pt./dec and a 5 s measuring point duration. The tests were conducted in both ramp-up and ramp-down to assess potential time-dependent behavior of the fluids. During analysis, the temperature was held constant by the fluid circulator at the different selected temperatures (in a range between  $10 \text{ }^\circ\text{C}$  and  $90 \text{ }^\circ\text{C}$ ).

2. Flow curve measurements in the on-state conditions were conducted using only the parallel-plate (PP) system compatible with the magnetocell. The magnetic field was varied from 0 T to 0.9 T, the maximum achievable magnetization using the inset plate and spacer ring in the magnetocell. Figure 5 illustrates the corresponding flux density achieved at each selected stimulation current. As expected, in the presence of the MRF, magnetization slightly increased due to the metal particles bridging the air gap between the yokes. Indeed, the maximum possible magnetization depends also on the gap height; at larger height, a lower magnetization density is reached due to the increase in the air gap filled with the MRF. For each selected magnetic field strength, a flow curve test was performed following the same procedure described above for tests performed in off-state mode. After pre-shearing, the magnetic field was applied in static conditions for 30 s to allow the formation of field-induced structures. Given that the response time of MR fluids is only a few milliseconds, allowing a significantly longer time should be sufficient to ensure the stable formation of field-induced structures. The test was then carried out by step increasing the shear rate logarithmically from  $1 \text{ s}^{-1}$  to  $1000 \text{ s}^{-1}$ , with 20 points per decade and a measurement duration of 5 s per point. Measurements were taken during both the ramp-up and ramp-down phases to assess any time-dependent properties of the fluid. This test was essential to study the field-dependent viscosity and yield stress in flow condition behavior of the material as a function of the applied field, temperature of analysis, and gap height. Since the instrument in this case was shear rate controlled, the material properties were evaluated in a continuous rotation of the spindle that can be defined as a dynamic condition.
3. Controlled shear stress tests were conducted to evaluate the yield stress of the MRF, starting from a static condition and applying a controlled shear stress ramp, determining the torque required to initiate viscous flow. The test was performed in a condition that could be defined as static, as the instrument was torque controlled in this case; therefore, the rotation is just a consequence of the applied torque, and the material properties were evaluated only in the range where no flow was observed. The parallel-plate (PP) system with the magnetocell was used, maintaining a fixed gap height of 1 mm and a fluid volume of  $400 \text{ }\mu\text{L}$ . Before each test, the sample was pre-sheared at  $20 \text{ s}^{-1}$  for 1 min, followed by a 30 s resting period at the desired magnetic flux density to allow equilibrium structure formation. During the measurement, shear stress was increased logarithmically from 1 kPa to 50 kPa, while strain was continuously recorded, with each measuring point set to 5 s. No specific number of points per decade was defined. Once the static yield point was exceeded, a sudden increase in the strain curve was observed due to the breakdown of the magnetic structures. The test was terminated when strain exceeded 1000%.

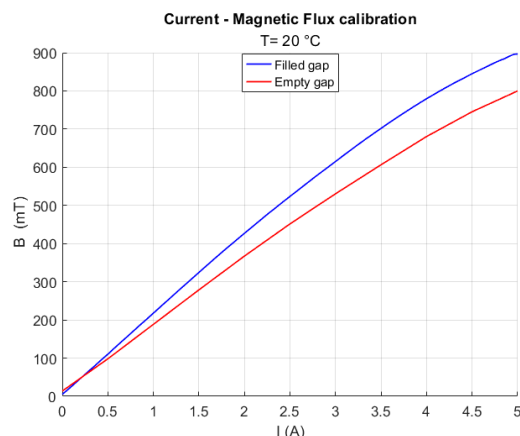


**Figure 5.** Calibration curve measured for the magnetocell with empty gap (red curve) and MRF-filled gap 0.9 mm (blue curve).

### 2.6. Data Correction for Parallel-Plate System

The measured rheological properties of the MRF obtained with a PP geometry were determined at the rim of the plate. The measured apparent shear stress ( $\tau_{aR}$ ) obtained is valid for Newtonian fluid and requires correction to obtain the true shear stress ( $\tau_R$ ) for a non-Newtonian fluid. Full description of the correction expression can be found in [14,18]; the short expression is shown here in Equation (1):

$$\tau_{aR} = \frac{2T}{\pi R^3} \rightarrow \tau_R = \tau_{aR} \left( \frac{3 + n'}{4} \right); n' = \frac{d(\log T)}{d(\log \dot{\gamma}_R)} \tag{1}$$

where T represents the measured torque and  $\dot{\gamma}_R$  is the true rim shear rate. From our experimental data, the correction factor consistently ranged between 0.7 and 0.8, leading to an average overestimation of the shear stress by approximately 25%. This indicates that analyses based on apparent parameters without correction are significantly flawed and yield inaccurate results.

## 3. Results and Discussion

### 3.1. Validation of Experimental Procedures

Initial validation tests were conducted on the measurement instrument to ensure the reliability and accuracy of the data obtained according to the experimental protocol defined for MRF testing. These tests were critical in determining the instrument’s performance characteristics, including sensitivity, precision, and repeatability, which are essential for consistent data analysis and comparison. During this phase, potential sources of error were also identified, such as fluid spillage, improper shear rate ramp velocity, fluid separation during extended tests, data acquisition timing, and volume control. The validation process allowed for the refinement of the experimental procedure, resulting in a robust protocol that ensures confidence in the accuracy and repeatability of the results obtained for future analyses.

The initial experiments aimed to determine the optimal rheometric parameters, particularly regarding test duration, data acquisition points per decade, and measurement time per point. Tests began with a default setting, allowing the rheometer to autonomously determine the measurement time for each point once steady-state equilibrium was reached. This approach, however, often led to prolonged averaging times, especially problematic in the “on-state” conditions, in which extended testing could significantly raise the sample temperature, potentially compromising the results. Additional tests, assessed the time required to achieve steady-state conditions, concluding that a maximum average time of

5 s per point was sufficient for a flow curve test as described above. Selecting 20 points per decade allowed for comprehensive material property mapping across all relevant scales, optimizing both accuracy and efficiency by minimizing the total test duration without sacrificing data quality.

The first experiment shown was performed to understand how varying fluid volumes influence the flow behavior at a fixed gap of 0.7 mm. Figure 6 shows the flow curve analysis in the on state (a) and off state (b). For these tests, material behavior was observed under conditions of 0 and maximum magnetization of 0.85 T. The fluid volume was determined by weighing the MRF deposited on the inset plate before the analysis. As expected, increasing the volume of fluid between the plates increases the shear stress ( $\tau$ ) for both the off and on state. At maximum volume, a 22% increase in shear stress was recorded in both states, emphasizing the importance of accurate MRF volume dosing control to avoid inconsistent data. Additionally, the interpretation of the apparent shear stress without applying proper corrections can lead to significant errors. By using correction formula (1), the true shear stress was calculated and plotted (dashed line) against the measured shear stress (solid line). Without this correction, the true shear stress and yield stress in the on state could be overestimated by as much as 25%, whereas in the off state, the error was minimal, likely due to the nearly Newtonian behavior of the fluid when unmagnetized. This highlights the importance of accounting for volume control and applying proper corrections in MRF testing to ensure the accuracy of the results.

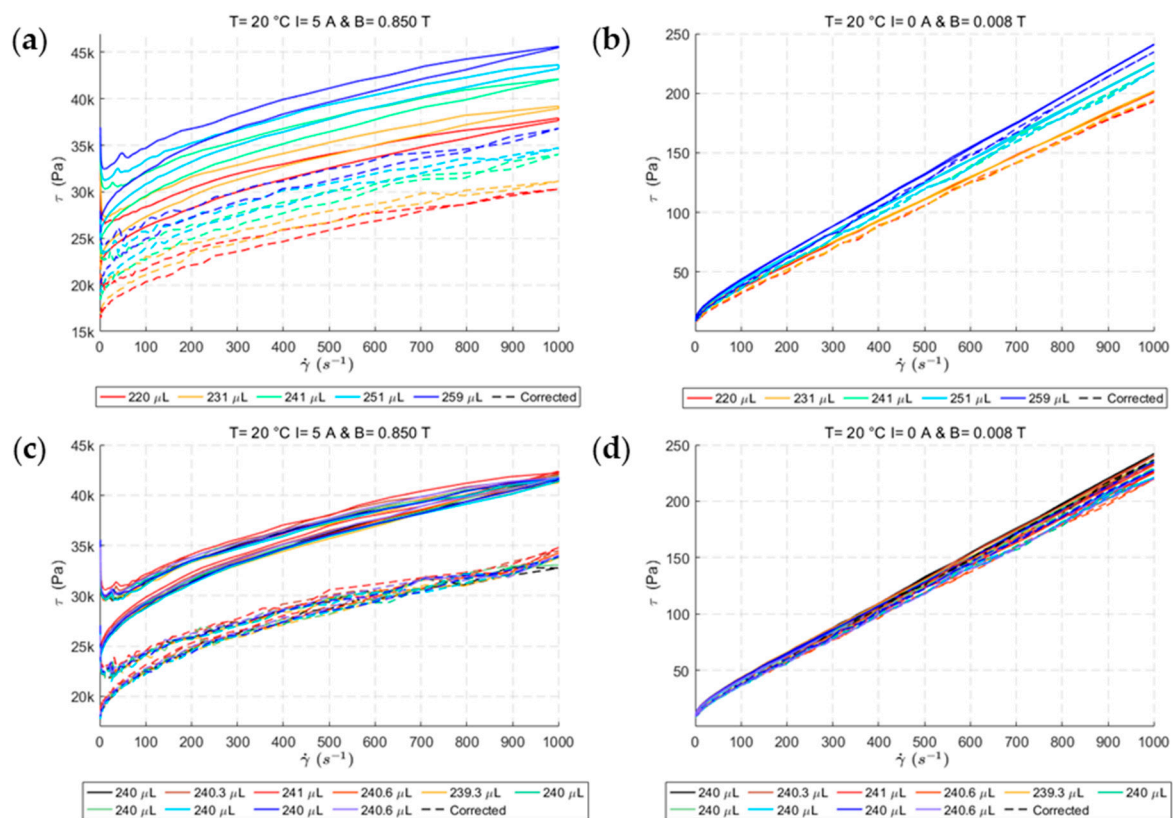


**Figure 6.** Flow curve performed at 0.7 mm gap: (a,b) shows the fluid volume characterization; solid lines are measured shear stress values, dotted lines are data after correction; (c,d) show the ten repetitions of the same test for both maximum magnetization (0.85 T) and off-state flow to understand test repeatability.

The second key experiment focused on evaluating the repeatability of the analysis. Using a fixed fluid volume, the same flow curve test was repeated ten times to assess the consistency of the measurements. Figure 6c,d present the results for the on-state and

off-state conditions, respectively. In both cases, the data demonstrated high consistency across the ten repetitions, as demonstrated also by the residual plot in Figure 7. It shows a mean deviation of the shear stress from the average shear stress curve calculated from the ten repetitions, below 3.45% for 0 T and 1.01% for 0.85 T. At 0 T in the low shear rate range ( $<10^1 \text{ s}^{-1}$ ), a larger deviation is observed due to the sensibility limit of the rheometer, which could induce a larger deviation in the data.

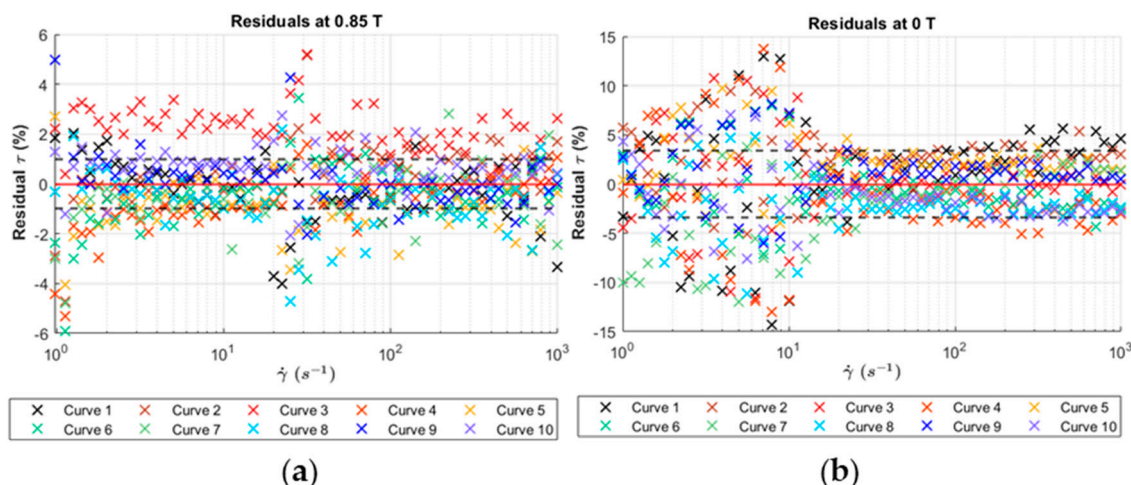


**Figure 7.** Residual plot for consistency of experiment repetitions: (a) maximum magnetization and (b) off state. The dotted line represents the average mean residue: 3.45% for 0 T and 1.01% for 0.85 T.

At maximum magnetization, it can be observed that the data series (curve 3) stands out compared with the other residuals. This series corresponds to repetition 3, during which 241  $\mu\text{L}$  of fluids were poured into the rheometer. The slightly larger amount of fluid used in this repetition may have caused a marginal increase in the shear stress, reflected as a residual value above the average.

The second test also emphasizes the necessity of a high accuracy of volume control for test repeatability as well as demonstrating the reliability of the experimental protocol.

### 3.2. Gap Height Characterization in Shear Condition

The initial MRF characterization focused on evaluating how the material performance varied by changing the gap heights. A flow curve test was conducted in both the off-state and the on-state mode (at 5 A/0.85 T) under an equilibrium temperature of 20 °C. The plotted curves represent the corrected shear stress values, as described by Equation (1), to ensure accurate analysis. Each test was repeated ten times for every gap height, and a mean curve was calculated and plotted (Figure 8) with the standard deviation displayed as error bars. This approach ensured statistical reliability in the results. For each gap, the fluid volume was selected following the procedure in Section 3.1: 0.21 mL, 0.24 mL, 0.27 mL, 0.30 mL, and 0.35 mL, respectively, for the 0.6 mm, 0.7 mm, 0.8 mm, 0.9 mm, and 1 mm gaps.

From the upward curve of each test, the dynamic yield stress ( $\tau_y$ ) and plastic viscosity ( $\eta_p$ ) were extracted by fitting the data to the Bingham model, presented in Equation (2):

$$\tau = \tau_y + \eta_p \dot{\gamma} \tag{2}$$

This method allows for an accurate description of the fluid’s behavior under different magnetic field conditions and gap settings, providing key insights into how these parameters influence both the yield stress and flow characteristics of the MRF. Figure 8 illustrates the results obtained for each gap. As expected, with the increasing gap and, consequently,

greater MRF volume at the maximum magnetization of 900 mT, the shear stress also rises. The curve displays the typical shape of an MRF, characterized by shear thinning as the shear rate increases. At  $1000 \text{ s}^{-1}$ , the shear stress reaches up to 38 kPa for the maximum height of 1 mm. For the off-state tests, the opposite trend is observed: as the gap increases, lower shear stress values are recorded. This is due to the wider spacing among the small metal particles, which allows more freedom of movement, thus reducing the formation of large friction forces.

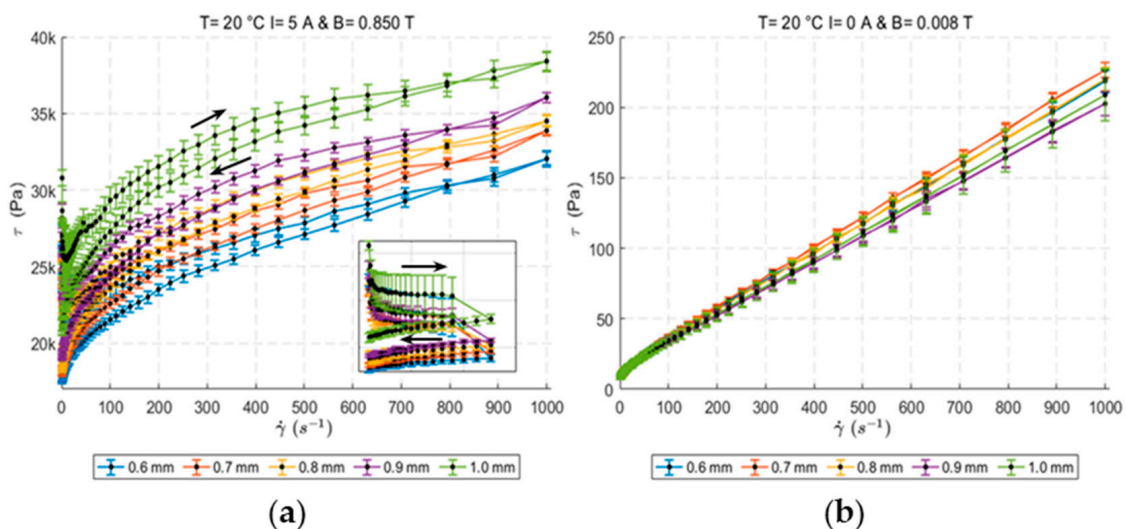


**Figure 8.** Flow curve experiments performed at different gap heights. (a) Max magnetization (900 mT); the inset shows a magnification of the initial part of the curves. (b) Zero magnetization. The black arrows indicate the ramp-up and -down curves for the green lines.

In this case, the curve resembles that of a Newtonian fluid, with a small yield point attributed primarily to the internal friction of the base oil and particles. The results confirm the expected behavior of MRFs in both magnetized and non-magnetized states, reinforcing the importance of precise control over gap height in real-world applications such as MR brakes, where both the yield stress and flow characteristics are crucial.

In order to interpret the experimental curves, the data for each gap were fitted using the Bingham model (Equation (2)), and the key parameters obtained from this modeling are summarized in Table 2. The yield stress shows an increasing trend with gap height, but this increase is not proportional. Up to 0.8 mm, the growth in yield stress is relatively modest. However, for the larger gaps (0.9 mm and 1 mm), a more pronounced increase is observed. This is likely due to the additional space allowing the magnetically induced chain-like structures more room to form larger and more robust structures, which during shear can generate higher torques. These findings underscore the complex interplay between gap height and MRF performance, where the structure of the fluid is strongly influenced by the available space for the formation of magnetic particle chains.

**Table 2.** Parameters obtained from the fit of the Bingham model to the up curve for each gap height. R-squared defines the accuracy of the model to adapt to the experimental data, while the correction parameter defines the percentage difference between the yield stresses obtained from corrected shear stress and from measured shear stress.

Gap (mm)	0.6	0.7	0.8	0.9	1
$\tau_y$ (Pa)	22,544	23,060	23,784	24,917	27,949
$R^2$	0.98	0.96	0.92	0.92	0.89
Correction (%)	26.7%	26.4%	25%	26.4%	25%

Another important aspect to take into account is the difference between the corrected and uncorrected shear stress data reported in Table 2, which shows the percentage difference between the real and apparent shear stress. Without the correction, the yield stress could be overestimated, on average, up to 25%, indicating that this is an essential step in data analysis.

Lastly, it is important to notice the difference in shear stress observed between the curves during the ramp-up and -down, as can be seen in Figure 8 and in more detail in the inset plot. It is a fundamental behavior to understand for the definition of a detailed card material in every shear range for the simulations. The up curve always shows an initial stress overshoot due to MRFs' viscoelasticity behavior when magnetized. This effect can be ascribed to multiple factors, including shear banding, which is due to non-uniform deformation causing the formation of multiple regions with different shear rates inside the material. The separation into multiple layers moving at different velocities can cause the formation of regions of higher stress causing overshoot followed by a decrease to the equilibrium condition [19]. Another well-explained cause, described in [14], is due to the formation of different mesostructures at different values of the Mason number under the influence of the external magnetic field in static or dynamic conditions. The Mason number (Mn) is a dimensionless parameter that characterizes the balance between viscous and magnetic forces in MRFs. It is directly proportional to the viscosity and shear rate, while it is inversely proportional to the magnetic permeability of free space, the particles' magnetization, and to the applied magnetic field. The Mason number plays a critical role in understanding how the mesostructures of magnetic particles in an MRF evolve under different flow conditions and applied magnetic fields. In low Mason numbers ( $< 1$ ), the magnetic forces are dominating over the viscous forces, leading to the formation of strong columnar mesostructures. This behavior can be observed in the very initial region (up-curve) of the rheogram at a low shear rate, where the dominant magnetic forces cause an initial step increase in the stress. By increasing the shear rate, the viscous forces start dominating with high Mason numbers ( $> 1$ ); the mesostructure formed is unable to withstand the shear forces, causing a complete rupture of the formed chain into a formation of sheetlike structures. Inducing a dynamic constantly forming and breaking, this results in a reduction in the yield stress generated, as can be seen from the down-ramp, reaching a significantly lower value of shear stress. For these reasons, it is crucial to study the material's behavior in both the up curve, beginning from a stable equilibrium with no imposed flow, and the down curve, where the material transitions from a flowing state back to a stationary condition ( $\dot{\gamma} = 0$ ). This approach provides insight into both the material's initial response to shear and its recovery or relaxation behavior when flow ceases.

### *3.3. Flow Curve Analysis Across a Broad Temperature Spectrum*

In this section, the analysis conducted at temperatures ranging from 10 °C to 90 °C, using both CP and PP systems, is presented. The cone-plate system, due to its larger surface area, allows for more accurate measurements of low viscosity values at high temperatures. This setup enables precise temperature control through the integration of a Peltier plate and hood, ensuring stable and uniform thermal conditions during the experiments. As a result, the CP system provides enhanced reliability in characterizing the off-state temperature-dependent rheological behavior of the MRF. Since the PP needs to be used for the on-state characterization, a comparison also in the off state was made to highlight potential differences between the two measuring systems.

### 3.3.1. Off-State Characterization with CP Geometry

The temperature-dependent viscosity behavior of the MRF was studied using cone-plate geometry for greater measurement accuracy. Before testing, the system was allowed to reach thermal equilibrium over a 20–30 min period. After loading the fluid sample, an additional 15 min waiting time was given to ensure the sample itself was thermally equilibrated. The test was conducted over a shear rate ranging from 0 s<sup>-1</sup> to 1500 s<sup>-1</sup>, with temperatures varying from 20 °C to 90 °C, to replicate the expected operational range in real-world applications. Higher temperatures were not tested, to prevent thermal degradation of the fluid, which was outside the scope of this study. Figure 9 presents the measured viscosities. Initially, at low shear rates, due to the high low-shear-rate viscosity ( $\eta_0$ ), the material shows a low yielding point. This is likely influenced by the metal particles, which, although not magnetized, can still increase the resistance to flow during the initial shear.

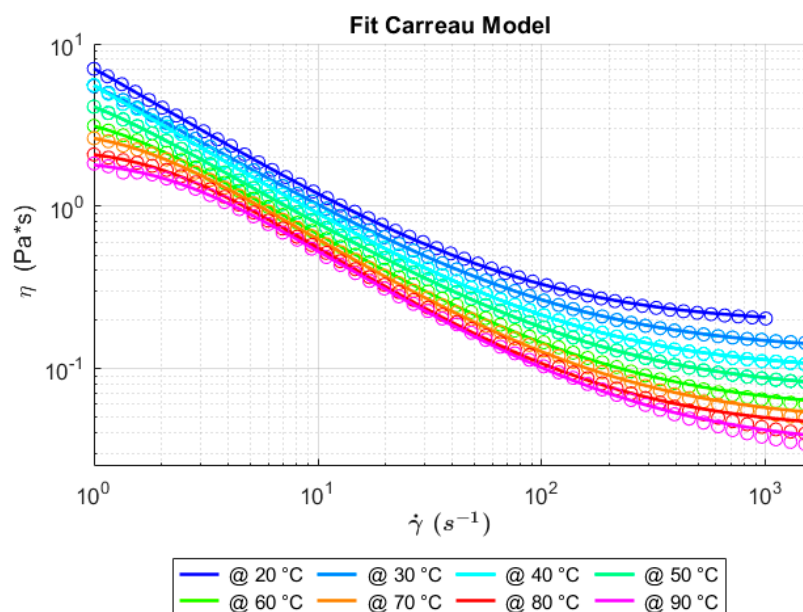


**Figure 9.** Viscosity curves measured at various temperatures in a shear rate range between 1 and 1500 s<sup>-1</sup>. Measuring geometry of the cone plate (50 mm in diameter, 0.998° angle) with a fixed gap of 0.1 mm and a fluid volume of 570 μL. Data fitted with the Carreau model.

Additionally, the additives used to minimize sedimentation likely contribute to the thickening of the base oil, further raising the initial viscosity. As the shear rate increases, viscosity decreases significantly, following the typical trend of a shear-thinning material, until a steady state is reached near the maximum shear rate. As temperature increases, a noticeable decrease in overall viscosity is observed, attributed to the thermal dependency of the viscosity reducing the internal friction within the fluid, which is typical for MRFs. This is also due to the thermal expansion of the oil, which reduces its volume fraction, leading to a further decrease in viscosity at elevated temperatures. The viscosity at very high shear rates ( $\eta_{\max\dot{\gamma}}$ ) and the low-shear-rate viscosity ( $\eta_0$ ) were determined by fitting the curves with the Carreau model (Equation (3)), which accurately describes the experimental curves.

$$\eta = \eta_\infty + \frac{\eta_0 - \eta_\infty}{\left(1 + (K\dot{\gamma})^2\right)^{\frac{m}{2}}} \tag{3}$$

Only for the 80 °C and 90 °C curves does the model deviate slightly from the data at high shear rates. This can be due to the combined high rotational speed and high

temperature, which can cause a loss of MRF from the measuring plates with a consequent decrease in the measured viscosity.

The rheological parameters obtained with the CP system are summarized in Table 3.

**Table 3.** Rheological parameters obtained from the Carreau model for CP analysis over different temperatures, high-shear-rate viscosity ( $\eta_{\max\dot{\gamma}}$ ), and low-shear-rate viscosity ( $\eta_0$ ).

T (°C)	20	30	40	50	60	70	80	90
$\eta_{\max\dot{\gamma}}$ (Pa·s)	0.186	0.128	0.096	0.071	0.054	0.046	0.041	0.032
$\eta_0$ (Pa·s)	21.24	10.58	8.22	6.52	3.98	3.07	2.30	1.95

### 3.3.2. On- and Off-State Characterization with PP Geometry

The temperature dependence of the MRF was also evaluated using the PP geometry in both the off and on states to compare the two measuring systems and assess the temperature's influence on the magnetized material. Temperature control for the magnetocell was managed solely by an external fluid circulator due to the presence of electrical coils used to generate the magnetic field. However, the significant heat generated by the coils, combined with the less-efficient liquid-based temperature control system, made it challenging to maintain stable temperature conditions during testing. As a result, considerable temperature fluctuations were observed, particularly during prolonged measurements, which impacted the consistency of the data. To reduce, at the minimum, the errors arising from the temperature fluctuations, a longer equilibration time was used. The test was performed in a lower shear rate range ( $0 \text{ s}^{-1}$  to  $1000 \text{ s}^{-1}$ ) with respect to the CP system, as above  $1000 \text{ s}^{-1}$ , fluid escapes from the gap, invalidating the test. This is due to the smaller spindle diameter that reaches a much higher rotational speed. A possible solution could be using a smaller gap.

Figure 10 shows the temperature influence on both the on and off states; in this case, the plotted curves refer to the apparent shear stress. At 900 mT, shown in (a) and (b), in general, the magnetic forces are predominant over the temperature influence on the viscous properties of the MRF. The viscosity curves indeed show minimal deviations across the increasing temperature. From the shear stress plot, as temperature increases, the stress curve is lowered, indicating that the thermal influence cannot be neglected.

This can be explained by a decrease in the magnetization induced by the temperature, lowering the magnetic forces that stabilize the field-induced structures. It can be attributed to multiple factors, including the lowering of the magnetic permeability of the metal powder that, by an increase in the thermal kinetic energy, causes the decrease in polarization capability of single domains. An increase in the metal particles' Brownian motion could reduce the stability of the field-induced structure formation, although in the selected T range, the thermal influence is not so prominent as to decrease the efficiency of the MRF, inducing possible safety issues in a real application. The observed variation in torque response includes the shear stress at maximum shear rate, decreased from 43 kPa to 37 kPa, and the "dynamic" yield stress, lowered from 30 kPa to 26 kPa.

The off-state measurement results closely matched those obtained using the CP system, displaying similar curve trends and temperature-dependent behavior, although the viscosities measured with the PP system were slightly higher across all temperatures. This discrepancy is likely due to the smaller radius of the PP plate, which is less optimal for off-state measurements. For low-viscosity fluids, larger surface areas or alternative geometries such as concentric cylinders or cone-plate systems are generally more suitable. Nevertheless, with appropriate data correction, off-state results from the PP geometry can still provide an accurate representation of the MRF's true rheological parameters.

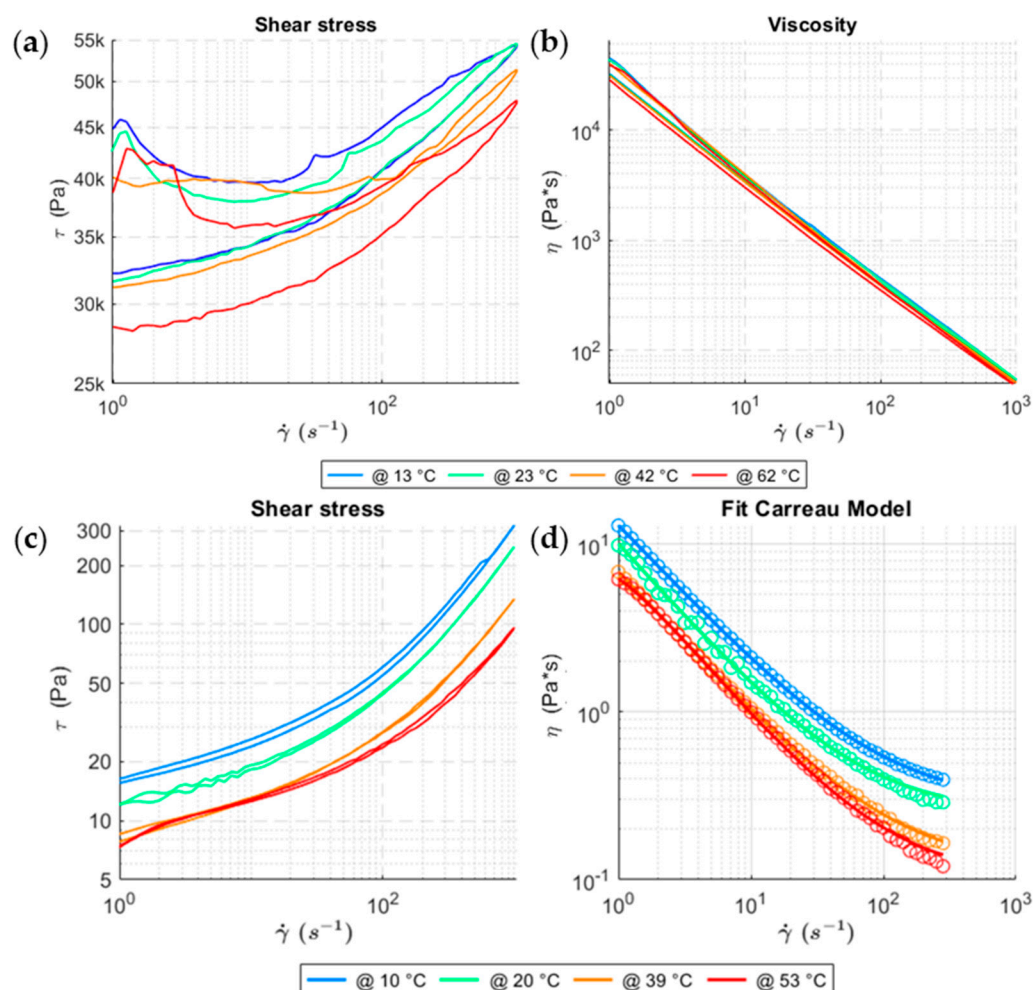


**Figure 10.** Apparent shear stress and viscosity curves measured at various temperatures in a shear rate range between 1 and 1000 s<sup>-1</sup>. Measuring geometry PP (20 mm diameter), 1 mm gap, 400 μL fluid volume. (a,b) max magnetization 900 mT flow curves, (c) off state shear stress, (d) viscosity curves fitted with the Carreau model for the extrapolation of high-shear-rate viscosity (data circles, line fit).

In Table 4, the rheological parameters obtained from the corrected data of the PP system are shown. In particular, the minimum viscosity in the off state was determined by fitting the corrected data with the Carreau model.

**Table 4.** MRF parameters obtained for the max magnetization and the off state for the PP geometry, corrected for the real shear stress: yield stress in the on state ( $\tau_{YD}$  900 mT), high-shear-rate viscosity for the off state ( $\eta_{max\dot{\gamma}}$  0 T), and maximum shear stress at the off state ( $\tau$  0 T).

T (°C)	10	20	40	60
$\tau_{YD}$ 900 mT (kPa)	30.1	28.6	26.9	26.4
$\eta_{max\dot{\gamma}}$ 0 T (Pa·s)	0.285	0.250	0.118	0.102
$\tau$ 0 T (Pa)	203	149	110	86

Comparing the off-state viscosities obtained at 40 °C, the results from the cone-plate system ( $\eta_{max\dot{\gamma} CP} = 0.096$  Pa·s) and the parallel-plate system ( $\eta_{max\dot{\gamma} PP} = 0.118$  Pa·s) closely match the supplier’s reported value of 0.112 Pa·s. The discrepancies of 12.5% for the CP system and 6.25% for the PP system are minor and fall within acceptable measurement variation, indicating that the results are reliable and not indicative of any faulty measurements.

### 3.4. Flow Curve Analysis Across the Full Magnetic Field Range

To understand the material response in the full range of magnetic fields, multiple flow curves were performed at increasing fields. The plot shown in Figure 11 represents the five curves, measured between 0.2 and 0.85 T; the data were corrected following the method defined in Equation (1) and fitted with a non-Newtonian fluid model. At low magnetization (0.2 T), the MRF exhibits primarily liquid-like behavior, deviating from the modeled response at shear rates above  $10^2 \text{ s}^{-1}$ , where a plateau emerges. This suggests a limit to the stress the fluid can sustain under low-field conditions, which may result from limited particle chain formation.

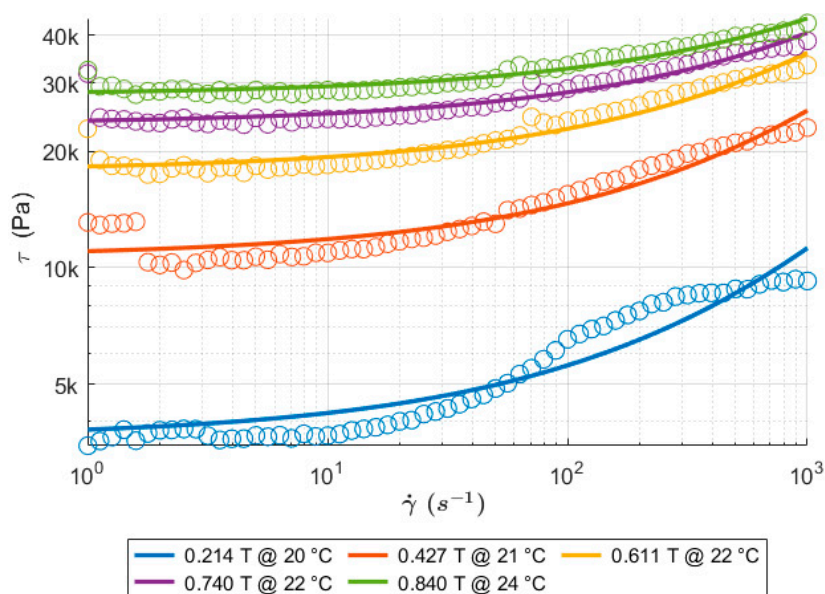


**Figure 11.** Flow curve analysis across the entire magnetic field range performed in a 1 mm gap (400  $\mu\text{L}$ ) between 1 and  $1000 \text{ s}^{-1}$ . Circles represent the experimental data, and the line represents the fitted non-Newtonian model. The test was performed with a starting equilibrium temperature of  $20 \text{ }^\circ\text{C}$ , and the reported temperature in the plot legend indicates the average temperature in the test.

However, as the magnetization increases to 0.4 T, the MRF’s response becomes more viscoelastic (solid-like), aligning closely with the model’s predictions. This shift in behavior reflects a more structured internal state, with particle chains forming stronger networks with higher resistance to shear. Further increases in the magnetic field cause a significant rise in the shear stress across all shear rates as well as an increase in the apparent yield stress, indicating that the MRF is transitioning toward a more solid-like state. The model-derived dynamic yield stress values for each field intensity are summarized in Table 5. Notably, as the magnetic field approaches the maximum intensity, the MRF’s shear stress step increase is lower, indicating a point where further magnetization gains yield minimal changes, likely due to reaching the metal particles’ magnetization saturation.

**Table 5.** Yield stress values obtained from the flow curves performed at different field values.

B (T)	0.214	0.427	0.611	0.740	0.840
$\tau_{YD}$ (kPa)	3.64	10.66	17.80	23.55	28.02

### 3.5. Controlled Shear Stress Test

A controlled-shear stress test was conducted at varying magnetization levels to evaluate the yield behavior of the MRF in the regime before flow initiation, which can be defined as measured in the “static” condition. In this test, shear stress was gradually increased

on a linear scale. Once the yield stress threshold was reached, the MRF transitioned from a solid-like state to a flowing state, resulting in a marked increase in shear rate. This rapid rate rise signifies the breakdown of the internal particle structure, enabling flow and providing a clear measure of the yield stress across different magnetic field intensities.

Figure 12 shows the stress increase for each magnetization level alongside the measured shear rate. Until no deformation is measured, the shear rate remains almost constant, at very small values in the  $10^{-3}$  to  $10^{-4}$  range. When the yielding point is reached, a large increase in the shear rate is measured, indicating the transition from a solid to a flowing regime. The applied stress was raised with a gradient of  $10.8 \text{ kPa}\cdot\text{s}^{-1}$ .

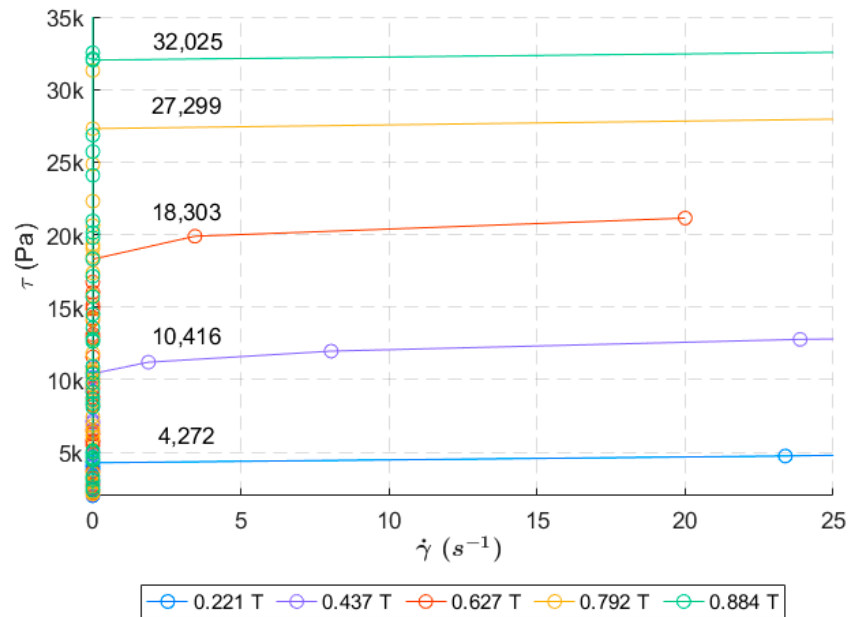


**Figure 12.** CSS test performed at 1 mm gap ( $400 \mu\text{L}$ ). The shear stress was increased logarithmically between 1 and 50 kPa with a stress increase gradient of  $10.8 \text{ kPa}\cdot\text{s}^{-1}$ ; when a large jump in the strain was recorded, the test was automatically stopped.

At low magnetization levels, the “static” yield stress was low, with the material transitioning to flow at minimal deformation (around 0.6% strain). As the field increased, the yield stress rose significantly: from 4 kPa at 0.22 T to 10 kPa at 0.44 T, 18 kPa at 0.63 T, 27 kPa at 0.79 T, and 32 kPa at 0.88 T. Higher magnetization also increased the material’s plastic deformation capacity, allowing it to withstand strain up to 10% before complete rupture of the particle chains. Unlike the previous flow tests, which measured yield stress in flow conditions, this test focused on static yield stress, an equilibrium parameter. The static yield stresses obtained are notably higher than their dynamic counterparts, reflecting the increased structural resilience of the MRF under static, equilibrium conditions before flow initiation. Table 6 reports the percentage difference between the dynamic and static yield stress values.

**Table 6.** Comparison of the percentage difference between the “static” and “dynamic” yield stresses for each magnetization.

B (T)	0.2	0.4	0.6	0.7	0.8
$\frac{\tau_{YD}}{\tau_{YS}}$ (%)	40.9	36.0	24.6	14.8	10.0

It is very interesting to observe the large viscous influence on the dynamical yield stresses, causing large decreases in the yielding capacity of the MRF. The significant dif-

ferences between the yield stresses measured in static and dynamic conditions, with the dynamic value being up to 40% lower, reflects the typical behavior of magnetorheological fluids (MRFs). In static conditions, the fluid is in an equilibrium state where magnetic particle chains are fully formed, offering maximum resistance to movement. In dynamic conditions, however, the continuous application of shear stress causes constant breaking and reformation of these particle chains, reducing the overall resistance of the material. This phenomenon explains the lower dynamic yield stress and highlights the importance of considering both parameters to fully characterize the behavior of an MRF, especially in applications such as braking systems, where static and dynamic conditions alternate.

#### 4. Conclusions

In conclusion, this study presents a comprehensive rheological analysis of magnetorheological fluids across key parameters such as magnetic field intensity, temperature, fluid volume, and shear rate. By examining both static and dynamic yield stress behaviors, significant insights were gained into the material's complex rheological profile. Experiments were performed with both cone-plate and parallel-plate geometries to optimize measurement accuracy for varying viscosities, confirming that each geometry contributes unique advantages in MRF testing. The cone-plate system provided high precision at low viscosities, while the parallel-plate configuration allowed controlled magnetization, though it resulted in slightly higher measured viscosities due to geometry effects. Temperature dependency analysis further demonstrated that viscosity and yield stress decline with increasing temperature, stressing the need for stable base oils and additives for high-temperature applications. Finally, the study confirms that small variations in fluid volume or particle concentration can drastically alter the rheological parameters, highlighting the criticality of precise dosing and sample preparation. The validated experimental protocol and corrected data analysis methods outlined here provide a solid foundation for future MRF studies, offering a detailed guideline for improving performance and reliability in MRF-based applications.

##### *Future Developments*

Colloidal stability, being one of the most critical properties of MR fluids, will be the primary focus of future tests. These tests will explore the potential for comparing different fluids and evaluating the long-term durability of the materials.

**Author Contributions:** Conceptualization, G.P., L.T. and G.I.; methodology, G.P.; validation, G.P.; formal analysis, G.P.; investigation, G.P.; data curation, G.P.; writing—original draft preparation, G.P.; writing—review and editing, L.T., G.I., H.d.C.P. and R.S.; supervision, L.T. and H.d.C.P.; resources, G.I., H.d.C.P. and E.S.; project administration, G.I. and H.d.C.P.; funding acquisition, G.I. and H.d.C.P. All authors have read and agreed to the published version of the manuscript.

**Funding:** This research was funded by the Programma NODES-Nord Ovest Digitale E Sostenibile (Grant agreement Cod. n.ECS00000036) del finanziato dal MUR sui fondi M4C2 –MISSIONE 4 COMPONENTE 2, “Dalla ricerca all’impresa” INVESTIMENTO 1.5, avviso “Ecosistemi dell’innovazione” nell’ambito del PNRR finanziato dall’Unione europea NextGenerationEU—Bando PoC Accademici a valere sui fondi CUPE13B22000020001–Spoke-2–“MATERIALIZED”.

**Data Availability Statement:** The raw data supporting the conclusions of this article will be made available by the authors on request.

**Conflicts of Interest:** The authors declare no conflicts of interest.

## References

1. Olabi, A.G.; Grunwald, A. Design and Application of Magneto-Rheological Fluid. *Mater. Des.* **2007**, *28*, 2658–2664. [[CrossRef](#)]
2. Laun, H.M.; Gabriel, C. Measurement Modes of the Response Time of a Magneto-Rheological Fluid (MRF) for Changing Magnetic Flux Density. *Rheol. Acta* **2007**, *46*, 665–676. [[CrossRef](#)]
3. Kubík, M.; Válek, J.; Žáček, J.; Jeniš, F.; Borin, D.; Strecker, Z.; Mazúrek, I. Transient Response of Magnetorheological Fluid on Rapid Change of Magnetic Field in Shear Mode. *Sci. Rep.* **2022**, *12*, 10612. [[CrossRef](#)] [[PubMed](#)]
4. Imberti, G.; de Carvalho Pinheiro, H.; Carello, M. MPS Analysis of Magneto-Rheological Fluid Magnetization Anisotropies. In Proceedings of the 2023 IEEE Vehicle Power and Propulsion Conference (VPPC), Milan, Italy, 24–27 October 2023; p. 6.
5. Kumar, V.; Kumar, R.; Kumar, H. Rheological Characterization and Performance Evaluation of Magnetorheological Finishing Fluid. *J. Appl. Fluid Mech.* **2020**, *13*, 185–197. [[CrossRef](#)]
6. Acharya, S.; Shyam Saini Tak, R.; Bhanu Singh, S.; Kumar, H. Characterization of Magnetorheological Brake Utilizing Synthesized and Commercial Fluids. *Mater. Today Proc.* **2021**, *46*, 9419–9424. [[CrossRef](#)]
7. Tsujita, T.; Ohara, M.; Sase, K.; Konno, A.; Nakayama, M.; Abe, K.; Uchiyama, M. Development of a Haptic Interface Using MR Fluid for Displaying Cutting Forces of Soft Tissues. In Proceedings of the 2012 IEEE International Conference on Robotics and Automation, Saint Paul, MN, USA, 14–18 May 2012; pp. 1044–1049.
8. Jonsdottir, F.; Thorarinsson, E.T.; Pálsson, H.; Gudmundsson, K.H. Influence of Parameter Variations on the Braking Torque of a Magnetorheological Prosthetic Knee. *J. Intell. Mater. Syst. Struct.* **2009**, *20*, 659–667. [[CrossRef](#)]
9. Imberti, G.; De Carvalho Pinheiro, H.; Carello, M. Design of an Innovative Zero-Emissions Braking System for Vehicles. In Proceedings of the 2022 International Conference on Electrical, Computer, Communications and Mechatronics Engineering (ICECCME), Male, Maldives, 16–18 November 2022; pp. 1–6.
10. Rwei, S.-P.; Shiu, J.-W.; Sasikumar, R.; Hsueh, H.-C. Characterization and Preparation of Carbonyl Iron-Based High Magnetic Fluids Stabilized by the Addition of Fumed Silica. *J. Solid State Chem.* **2019**, *274*, 308–314. [[CrossRef](#)]
11. Eshgarf, H.; Ahmadi Nadooshan, A.; Raisi, A. An Overview on Properties and Applications of Magnetorheological Fluids: Dampers, Batteries, Valves and Brakes. *J. Energy Storage* **2022**, *50*, 104648. [[CrossRef](#)]
12. Osial, M.; Pregowska, A.; Warczak, M.; Michael, G. Magnetorheological Fluids: A Concise Review of Composition, Physicochemical Properties, and Models. *J. Intell. Mater. Syst. Struct.* **2023**, *34*, 1864–1884. [[CrossRef](#)]
13. Jolly, M.R.; Bender, J.W.; Carlson, J.D. Properties and Applications of Commercial Magnetorheological Fluids. *J. Intell. Mater. Syst. Struct.* **1999**, *10*, 5–13. [[CrossRef](#)]
14. Bossis, G.; Volkova, O.; Lācis, S.; Meunier, A. Magnetorheology: Fluids, Structures and Rheology. In *Ferrofluids*; Springer: Berlin/Heidelberg, Germany, 2002; Volume 594, pp. 202–230. ISBN 978-3-540-43978-3.
15. Carlson, J.D. What Makes a Good MR Fluid? *J. Intell. Mater. Syst. Struct.* **2002**, *13*, 431–435. [[CrossRef](#)]
16. Laun, H.M.; Schmidt, G.; Gabriel, C.; Kieburg, C. Reliable Plate–Plate MRF Magnetorheometry Based on Validated Radial Magnetic Flux Density Profile Simulations. *Rheol. Acta* **2008**, *47*, 1049–1059. [[CrossRef](#)]
17. Gabriel, C.; Kieburg, C.; Laun, H.M. Clutch and Brake Related Testing of Magnetorheological Fluids Using the Basf Twin Gap Magnetocell. *Appl. Rheol.* **2010**, *20*, 41778. [[CrossRef](#)]
18. Jonkkari, I.; Kostamo, E.; Kostamo, J.; Syrjala, S.; Pietola, M. Effect of the Plate Surface Characteristics and Gap Height on Yield Stresses of a Magnetorheological Fluid. *Smart Mater. Struct.* **2012**, *21*, 075030. [[CrossRef](#)]
19. Delgado, M.A.; Secouard, S.; Valencia, C.; Franco, J.M. On the Steady-State Flow and Yielding Behaviour of Lubricating Greases. *Fluids* **2019**, *4*, 6. [[CrossRef](#)]
20. Horak, W.; Stepien, B.; Sapiński, B. Experiments and Analysis of the Limit Stresses of a Magnetorheological Fluid. *Acta Mech. Autom.* **2022**, *16*, 408–416. [[CrossRef](#)]
21. Hemmatian, M.; Sedaghati, R.; Rakheja, S. Temperature Dependency of Magnetorheological Fluids' Properties under Varying Strain Amplitude and Rate. *J. Magn. Magn. Mater.* **2020**, *498*, 166109. [[CrossRef](#)]
22. Li, H.; Jönkkäri, I.; Sarlin, E.; Chen, F. Temperature Effects and Temperature-Dependent Constitutive Model of Magnetorheological Fluids. *Rheol. Acta* **2021**, *60*, 719–728. [[CrossRef](#)]
23. Imberti, G.; de Carvalho Pinheiro, H.; Carello, M. Impact of the Braking System Generated Pollutants on the Global Vehicle Emissions: A Review. In Proceedings of the New Developments in Environmental Science and Engineering; Chen, X., Ed.; Springer Nature: Singapore, 2024; pp. 11–19.
24. De Carvalho Pinheiro, H.; Carello, M.; Imberti, G.; Tempone, G. *Innovative Zero-Emissions Braking System: Performance Analysis Through a Transient Braking Model*; SAE International: Warrendale, PA, USA, 2024.
25. De Carvalho Pinheiro, H.; Imberti, G.; Carello, M. *Pre-Design and Feasibility Analysis of a Magneto-Rheological Braking System for Electric Vehicles*; SAE International: Warrendale, PA, USA, 2023.
26. Caushaj, S.; Imberti, G.; de Carvalho Pinheiro, H.; Carello, M. Electromagnetic Interaction Model between an Electric Motor and a Magnetorheological Brake. *Designs* **2024**, *8*, 25. [[CrossRef](#)]

27. Laun, H.M.; Gabriel, C.; Kieburg, C. Twin Gap Magnetorheometer Using Ferromagnetic Steel Plates—Performance and Validation. *J. Rheol.* **2010**, *54*, 327–354. [[CrossRef](#)]
28. Nguyen, Q.H.; Choi, S.B. Optimal Design of an Automotive Magnetorheological Brake Considering Geometric Dimensions and Zero-Field Friction Heat. *Smart Mater. Struct.* **2010**, *19*, 115024. [[CrossRef](#)]

**Disclaimer/Publisher’s Note:** The statements, opinions and data contained in all publications are solely those of the individual author(s) and contributor(s) and not of MDPI and/or the editor(s). MDPI and/or the editor(s) disclaim responsibility for any injury to people or property resulting from any ideas, methods, instructions or products referred to in the content.